

Article

Thermodynamic and Economic Evaluation of a Novel Green Methanol Poly-Generation System

Qiliang Ye ^{1,*}, Yipeng Bao ¹, Hui Pan ² , Yulan Liu ¹ and Peiqing Yuan ¹¹ School of Chemical Engineering, East China University of Science and Technology, Shanghai 200237, China² College of Environmental and Chemical Engineering, Shanghai University of Electric Power, Shanghai 200090, China

* Correspondence: yql@ecust.edu.cn

Abstract: Methanol is considered a sustainable alternative energy source due to its ease of storage and high-octane rating. However, the conventional methanol production process is accompanied by resource consumption and significant greenhouse gas emissions. The electrochemical reaction of electrochemically reacted hydrogen (H₂) with captured carbon dioxide (CO₂) offers an alternative route to methanol production. This paper presents a new green poly-generation system consisting of a parabolic trough solar collector (PTC) unit, an organic Rankine cycle (ORC) unit, a CO₂ capture unit, an alkaline electrolysis unit, a green methanol synthesis and distillation unit, and a double-effect lithium bromide absorption refrigeration (ARC) unit. The system mainly produced 147.4 kmol/h of methanol at 99.9% purity, 283,500 kmol/h of domestic hot water, and a cooling load of 1341 kW. A total 361.34 MW of thermal energy was supplied to the ORC by the PTC. The alkaline electrolysis unit generated 464.2 kmol/h of H₂ and 230.6 kmol/h of oxygen (O₂) while providing H₂ for methanol synthesis. Thermodynamic and economic analysis of the system was carried out. The energy and exergy efficiency of the whole system could reach 76% and 22.8%, respectively. The internal rate of return (IRR) for the system without subsidies was 11.394%. The analysis for the methanol price showed that the system was economically viable when the methanol price exceeded \$363.34/ton. This new proposed poly-generation system offers more options for efficiently green methanol production.

Keywords: green methanol; thermo-economic analysis; CO₂ capture; process simulation



Citation: Ye, Q.; Bao, Y.; Pan, H.; Liu, Y.; Yuan, P. Thermodynamic and Economic Evaluation of a Novel Green Methanol Poly-Generation System. *Processes* **2023**, *11*, 206. <https://doi.org/10.3390/pr11010206>

Academic Editor: Andrew S. Paluch

Received: 13 December 2022

Revised: 26 December 2022

Accepted: 7 January 2023

Published: 9 January 2023



Copyright: © 2023 by the authors. Licensee MDPI, Basel, Switzerland. This article is an open access article distributed under the terms and conditions of the Creative Commons Attribution (CC BY) license (<https://creativecommons.org/licenses/by/4.0/>).

1. Introduction

Since the first industrial revolution, fossil fuels have been the primary source of energy for numerous economic sectors. They may still play an essential role in this century. However, burning fossil fuels has intensified greenhouse gases such as CO₂ emissions. The concentration of CO₂ in the atmosphere has increased by 30% compared to before industrialization. It is estimated that carbon dioxide emissions will reach about 26 billion tons per year by 2100 [1]. The continuous increase of carbon emissions will adversely affect the global environment, such as global warming, glacier melting, climate anomalies, sea level rise, and continental inundation [2]. According to the Intergovernmental Panel on Climate Change (IPCC), global warming may be reduced to 1.5 °C by various mitigation measures, consequently reducing energy and resource intensity, improving decarbonization rates, and encouraging carbon capture systems [3].

The development of green energy sources has made it possible to reduce carbon emissions. Typical green energy sources include mainly solar, wind, and biomass, providing additional options for producing many chemical products [4]. Methanol has gradually been recognized by the global industry as a new clean and renewable fuel due to its wide range of sources, huge economic volume, and sustainable development of the whole industry chain [5]. Global methanol production is expected to increase to 1.9 million tons per year by 2030, and more than 80% of methanol is produced by reforming natural gas with

steam. Nevertheless, this process is accompanied by enormous greenhouse gas emissions. However, this process is accompanied by huge carbon emissions. Catalytic hydrogenation of CO₂ to green methanol provides an alternative route to methanol production [6]. As the primary raw material, the cost of hydrogen has become one of the crucial factors restricting CO₂ hydrogenation to methanol. Hydrogen from electrolytic water is an environmentally friendly method that reduces dependence on fossil fuels. In a future clean energy system, electricity and hydrogen can be used as complementary energy carriers, as electricity can easily be converted into hydrogen and vice versa [7]. Green energy generation is a clean and viable way to produce hydrogen from water electrolysis.

Solar energy is the most popular green energy source that can be converted into thermal and electrical energy [8,9]. The primary benefit of solar energy is its global availability with varying intensities [10]. Solar collectors come in two common types produce heat energy after absorbing and transferring light from the sun to the fluid inside the collector [11]. PTC is a typical form of concentrator utilized in solar facilities. They include a reflector in the shape of a parabola, a tubular receiver, a support structure, and a tracking structure [12]. The collector reflects sunlight incoming rays to a tubular receiver containing a heat transfer fluid (HTF) to create heat for the ORC [13]. ORC is one of the power generation systems that utilize solar collector-generated heat [14].

Thus, the integration of technologies such as solar collectors, ORC, electrolytic water hydrogen production, CO₂ capture, and methanol synthesis can approach the goal of green methanol production and global carbon emission reduction. Mariano [15] developed an integrated framework for designing solar and wind energy storage in the form of methanol under uncertain conditions and conducted a case study to verify the feasibility of using renewable energy to participate profitably in the synthesis of methanol. El-Emam et al. [16] developed an innovative new integrated multi-generation energy structure comprised of a concentrated solar collector, ORC, ARC, electrolysis unit, and desalination unit. The thermodynamic analysis revealed that the process's maximum and minimum total furnace efficiencies were 39% and 21.7%, respectively. Mehrpooya et al. [17] developed an integrated solar-driven system with solar collectors, a desalination process, and ARC for freshwater production and cooling and performed a brane analysis and economic analysis. The results showed that the total efficiency of the process was 66.05% for the total radiation and 80.70% for the thermal efficiency. Liu et al. [18] designed and assessed an integrated process consisting of syngas purification, ORC, and ARC in terms of energy, watts, economy, and the environment. The performance analysis revealed that the system's overall fire efficiency was 42.88%. Xia et al. [19] suggested a coal-to-methanol process that combines CO₂ collection and ORC power generation. This process was simulated and studied from energy-saving and economic viewpoints. The energy efficiency of the proposed coal-to-methanol process combined ORC system was 45.5% at a carbon capture rate of 60%, with a payback time of 2.7 years. Chein et al. [20] studied the impact of various reactors and reactant ratios on methanol yield and carried out a comprehensive investigation of methanol synthesis performance based on thermodynamic equilibrium and kinetic models with captured CO₂ and synthesis gas generated from biogas as feedstock. Patrizio et al. [21] developed an integrated renewable energy electrolytic water hydrogen production, carbon capture, and methanol synthesis system with heat exchange analysis and techno-economic evaluation.

Catalytic hydrogenation of captured CO₂ to green methanol offers a new option for methanol production and meets the goal of sustainable development and global carbon neutrality. This paper proposes the system integration of PTC, ORC, CO₂ capture unit, alkaline electrolysis unit, green methanol synthesis and distillation unit, ARC, and for multi-cogeneration of useful commodities. Such a system will provide green methanol, electricity, O₂, domestic hot water, and cooling. It was thermodynamically analyzed by energy and exergy analysis. An economic analysis was also performed to evaluate the system's feasibility.

2. Process Simulation

Figure 1 shows the flow chart of the proposed green poly-generation integrated system. The proposed integrated system consists of six units: (1) PTC for supplying thermal energy required by the ORC; (2) ORC for power generation; (3) CO₂ capture unit; (4) alkaline electrolyzer for H₂ production; (5) green methanol synthesis and distillation unit; and (6) double-effect lithium bromide ARC unit for cooling production.

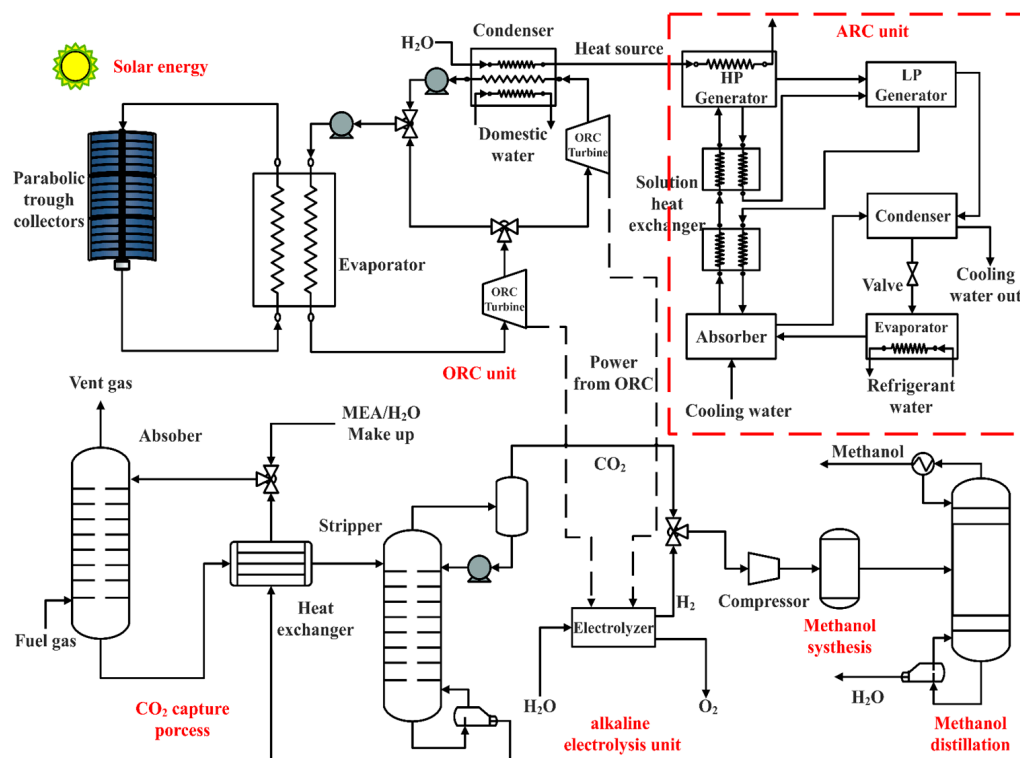


Figure 1. Flow chart of the proposed green poly-generation integrated system.

The sun was chosen as the main source of energy production. The PTC produces thermal energy after absorbing and transferring the sun's light energy to the heat transfer fluid inside the collector. The heat transfer fluid chosen for the study was Thermonil-VP1, which has a wide operating temperature range and uniform heat transfer. In addition, it provides precise temperature control and requires low maintenance costs, making it widely used in parabolic trough collector plants [13]. The thermal energy from the heat transfer fluid in the PTC provides the necessary thermal load through the evaporator for the ORC to generate electricity. The choice of working fluid significantly impacts the ORC which can effectively improve its efficiency. The electricity from the ORC is fed into an alkaline electrolyzer, which decomposes water into O₂ and H₂. 99.8% purity of H₂ is obtained in this way (with an efficiency of approximately 80%). The CO₂ capture unit was integrated into the system, and mono-ethanolamine (MEA) was selected as the gas absorber to capture CO₂, which has the advantages of fast reaction rate, low relative molecular mass, low cost, good thermal stability, and high absorption capacity [22]. The H₂ from the electrolyzer and the captured CO₂ are compressed and fed into the methanol synthesis unit, after which crude methanol can be synthesized in the presence of a synthesis catalyst. The crude methanol was dehydrated through the distillation column to obtain green methanol with a purity of 99.9%. Part of the domestic hot water was also provided through the ORC cycle, while the ORC also provided a heat source for the double-effect lithium bromide ARC for cooling production.

The block diagram of the proposed green poly-generation integrated system is shown in Figure 2: The PTC unit provided 361,354 kW of thermal energy as a heat source for the ORC unit, which generated a total of 44,902 kW of energy for internal consumption.

Instead, 37,285 kW of energy was used in an alkaline electrolyzer to produce 464.2 kmol/h of H₂, which was introduced into the green methanol synthesis unit along with CO₂. This system also had a water tank in which 25 °C water was used as an intermediate medium for thermal integration. Finally, the system produced a total of 147.4 kmol/h of green methanol, 230.6 kmol/h of O₂, 283,500 kmol/h of domestic hot water, and an additional 1341 kW of cooling as a by-product.

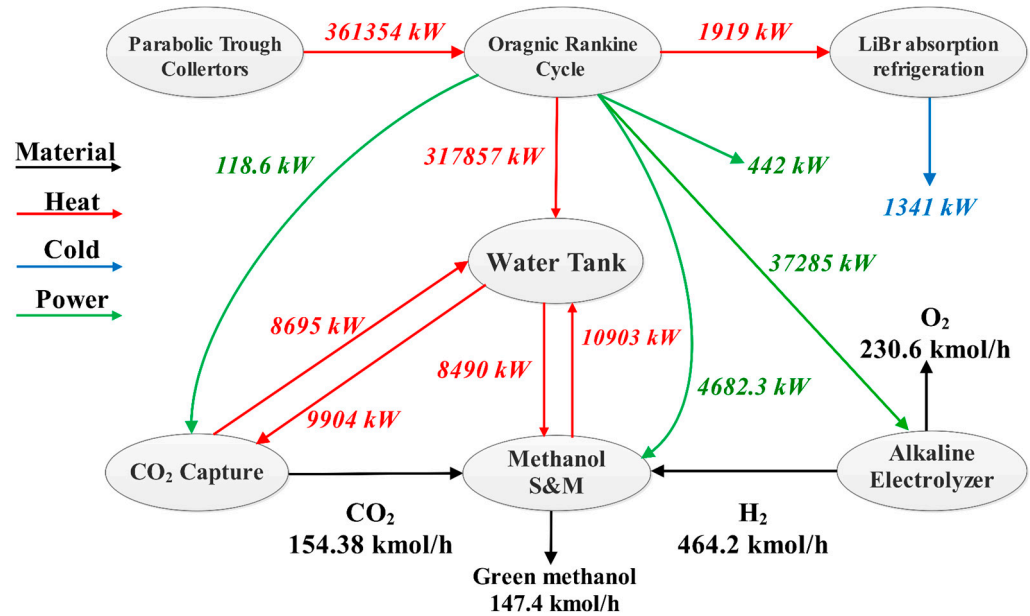


Figure 2. Block diagram of the proposed green poly-generation integrated system.

Aspen Plus and MATLAB were used to simulate the integrated system. The modeling and simulation of the system are detailed concisely and precisely in this section.

2.1. Parabolic Trough Collectors

This paper developed an energy balance model of the PTC system using a lumped thermal mathematical approach. The PTC was assumed to operate on a horizontal north-south axis, tracking the sun from east to west. The two main parameters for evaluating the collector performance were the thermal efficiency of the collector and the useful energy collected by the system, which can be calculated using Equations (1) and (3), respectively. The thermal efficiency of the PTC can be calculated by the following equation:

$$\eta = \frac{Q_u}{I_G A_a} \tag{1}$$

where Q_u was the useful energy collected by the system, I_G is the total radiation and A_a was the light-harvesting area. The total radiation depends on geographical features and was estimated as the following equation:

$$I_G = I_d + I_b \tag{2}$$

where I_b and I_d are normal radiation and diffuse radiation, respectively.

The useful energy collected by the system can be calculated by the following equation:

$$Q_u = \dot{m} C_p (T_{out} - T_{in}) \tag{3}$$

where T_{in} , T_{out} , C_p , and \dot{m} are the fluid inlet temperature, fluid outlet temperature, working fluid heat capacity, and mass flow rate, respectively. The equation does not allow for the observation of the effect of numerous constants, such as the coefficient of heat loss and the

optical efficiency of the collector. Therefore, a relational equation that considers the effect of heat loss and optical loss is as follows:

$$Q_u = F_R [I_G \eta_{opt} A_a - A_r U_L (T_{in} - T_a)] \quad (4)$$

where F_R , η_{opt} , and U_L are the heat dissipation coefficient, optical efficiency, and heat loss coefficient, respectively.

$$F_R = \frac{\dot{m} C_p}{A_r U_L} \left[1 - \exp\left(\frac{-A_r U_L F'}{m C_p}\right) \right] \quad (5)$$

$$U_L = \left[\frac{A_r}{A_c (h_a + h_b)} + \frac{1}{h_c} \right]^{-1} \quad (6)$$

where h_a , h_b , and h_c are the convective heat transfer coefficient between the cover and the air, the convective heat transfer coefficient between the external environment and the cover, and the convective heat transfer coefficient between the receiver and the cover, respectively, and calculated by the following equations.

$$h_a = \frac{8.6 V_{air}^{0.6}}{L^{0.4}} \quad (7)$$

$$h_b = \varepsilon_c \sigma (T_c^2 + T_{sky}^2) (T_c + T_{sky}) \quad (8)$$

$$h_c = \frac{\sigma (T_r^2 + T_c^2) (T_r + T_c)}{\frac{1}{\varepsilon_r} + \left(\frac{1}{\varepsilon_c} - 1\right) \frac{A_r}{A_c}} \quad (9)$$

where σ is the Stefan–Boltzmann constant, ε_r and ε_c are the emissivity of the receiver and the cover, respectively. T_c and T_r are the cover temperature and the receiver temperature, respectively.

For the convective heat transfer coefficient of the fluid in the tube, the Reynolds number and Nusselt number can be calculated by the following equations.

$$h_{HTF} = \frac{Nu K_{HTF}}{D_{abi}} \quad (10)$$

$$f = [1.82 \log_{10}(Re_{Dabi}) - 1.64]^{-2} \quad (11)$$

$$Nu = \frac{\left(\frac{f}{8}\right) (Re_{Dabi} - 1000) Pr_{HTF}}{1 + 12.7 \sqrt{\frac{f}{8}} \left(Pr_{HTF}^{\frac{2}{3}} - 1\right)} \left(\frac{Pr_{HTF}}{Pr_{abi}}\right)^{0.11} \quad (12)$$

$$Re = \frac{4\dot{m}}{\pi D_{abi} \mu} \quad (13)$$

where f is the friction coefficient of the inner wall of the collector, Re and Nu are the Reynolds number and Nusselt number, respectively.

The optical efficiency can be calculated by the following equation.

$$\eta_{opt} = \rho_{cl} \tau \alpha_a \gamma K_\theta X_{end} \quad (14)$$

$$X_{end} = 1 - \frac{f_L}{L} \tan \theta \quad (15)$$

where ρ_{cl} is the specular reflectance, τ is the cover transmittance, α_a is the heat absorbing tube surface absorbance, f_l is the intercept factor, K_θ is the angle of incidence modifier, X_{end} is the terminal loss, f_L is the parabolic focal length, and θ is the angle of incidence.

2.2. Organic Rankine Cycle

The ORC was modeled under the assumption that the thermal energy generated by the PTC supplied the required thermal load for the ORC with no losses. From the literature, ORC is one of the suitable methods to generate power from solar thermal sources [23]. As shown in Figure 1, the regenerative extraction ORC system proposed in this paper consists of an evaporator, a condenser, two pumps, and two gas turbines. The ORC energy output and efficiency are the two main parameters to evaluate its performance. The following equations can calculate the energy output of the ORC.

$$W_{orc} = W_{T_{orc}} - W_{P_{orc}} \quad (16)$$

$$W_{T_{orc}} = m_{orc}(h_{iT} - h_{oT}) \quad (17)$$

where $W_{T_{orc}}$ is the gas turbine output work, $W_{P_{orc}}$ is the pump power consumption, h denotes the enthalpy, the subscripts for T and P represent the gas turbine and pump, respectively.

The thermal efficiency of the ORC can be defined as the output power divided by the heat in the evaporator.

$$\eta_{orc} = \frac{W_{orc}}{Q_{evaporator}} \quad (18)$$

2.3. CO₂ Capture Unit

Carbon capture technology has been widely used to reduce greenhouse gas emissions on a large scale. The MEA-based CO₂ capture system supplies CO₂ to the green methanol synthesis and distillation unit. After the desulfurization and denitration processes, the flue gas (FGS) enters the absorber and contact the MEA solution. During this procedure, CO₂ is absorbed from the flue gas. Clean flue gas (vent gas) exits the absorber's upper portion. The MEA-lean solvent absorbs CO₂ and then becomes the MEA-rich solvent, which is pressurized by a pump and heated up by a rich-lean heat exchanger before entering the stripper.

In the stripper, the CO₂ in the MEA-rich solvent is reduced by the heating process. The decreased CO₂ exits from the top of the stripper, while the desorbed MEA solution escapes from the bottom of the stripper. The desorbed MEA solution is cooled by the rich-lean heat exchanger and mixed with more water before entering the absorber to begin the next cycle. The following operational parameters were considered to validate the model for the MEA-based CO₂ capture process.

CO₂ removal rate:

$$CRR = \frac{m_{CO_2out}}{m_{CO_2in}} \quad (19)$$

Specific regeneration heat duty:

$$q_{reb} = \frac{Q_{Exchanger}}{m_{CO_2out}} \quad (20)$$

Liquid solvent to flue gas ratio in the absorber:

$$\frac{L}{G} = \frac{m_{Solvent}}{m_{Fuel\ gas}} \quad (21)$$

Considering that an increase in MEA concentration can cause severe corrosion effects, a 30 wt.% MEA solution was chosen for this paper. The model developed in this paper was validated using the same input data as the NETL model [24]. The results comparing the operational parameters of the NETL data are presented in Table 1. The typical value of 90% CRR used to simulate the carbon capture process [25,26] and the design of the actual amine scrubber [27] was higher than the value of the reference unit used in the validation

model (71.3%). Therefore, this paper used a CRR of 80% as an intermediate value for the simulations. The desired CRR can be achieved by adjusting the mass flow rate of dilute MEA solvent. Thus, the absorber's ratio of liquid solvent to flue gas (L/G ratio) increases. The reliability of the MEA-based CO₂ capture system proposed in the study was verified.

Table 1. Validation of the developed CO₂ capture model.

Operating Parameter	NETL [24]	Developed Model
CRR	71.3	80.0
q _{reb} (kJ/g CO ₂)	6.05	6.18
L/G ratio	4.80	5.40

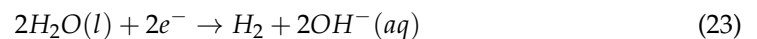
The detailed equilibrium constants for the controlled equilibrium ion reactions were employed using the literature [28]. It is worth noting that the reaction equilibrium constants are calculated as a function of temperature, as shown in Equation (22).

$$\ln(K_{eq}) = A + \frac{B}{T} + C \ln(T) + DT \quad (22)$$

2.4. Alkaline Electrolysis Unit

Alkaline electrolysis is considered a stable technology, with a service life of up to 15 years. At the same time, alkaline electrolyzers operate at high efficiencies, with typical values in the range of 47% to 82%. It is the most developed, accessible, and cost-effective method for low-temperature electrolysis on a commercial scale [29]. When a current is established between the positive and negative electrodes, hydrogen is released from the cathode, producing hydroxide anions circulated across the diaphragm to the anode within an electric field established by an external power source. The hydroxide anions recombine at the surface of the anode, producing O₂ and releasing electrons from the closed circuit. The anode, cathode, and overall reaction of the cell are as follows.

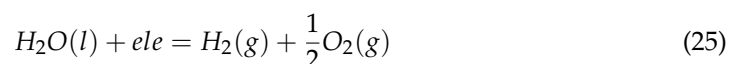
Anode:



Cathode:



Overall:



2.5. Green Methanol Synthesis and Distillation

The feed H₂ from the alkaline electrolyzer and the captured CO₂ are gradually compressed to 50 bar utilizing a multi-stage compressor into the reactor with a Cu/Zn/Al/Zr catalyst [30,31]. The reactor for CO₂ hydrogenation to methanol is a multi-tube catalytic reactor with tube dimensions of 12 m in length, 0.06 m in diameter, and a catalyst bed void ratio of 0.5 [32]. The detailed chemical reactions using the Cu/Zn/Al/Zr catalyst are shown in Table 2.

Table 2. Methanol synthesis reactions on the Cu/Zn/Al/Zr catalyst [30,31].

Reaction	Enthalpy Variation
CO + 2H ₂ ↔ CH ₃ OH	ΔH _{298 K} = −90.77 kJ/mol CO ₂
CO ₂ + H ₂ ↔ CO + H ₂ O	ΔH _{298 K} = +41.21 kJ/mol CO ₂
CO ₂ + 3H ₂ ↔ CH ₃ OH + H ₂ O	ΔH _{298 K} = −49.16 kJ/mol CO ₂

The reaction equilibrium constants k_A , k_B , and k_C were obtained from Lim et al. [33]. It is worth noting that the equilibrium constant data in the literature are in better agreement with the equilibrium constants calculated by Aspen Plus using the equilibrium reactor. The equilibrium constants were calculated as follows.

$$\ln k_A = -52.096 + \frac{11840}{T} \quad (26)$$

$$\ln k_B = 5.639 - \frac{5285}{T} \quad (27)$$

$$\ln k_C = -46.457 + \frac{6555}{T} \quad (28)$$

The kinetics of the methanol synthesis reaction are of the Langmuir–Hinshelwood (LHHW) form, with the reaction kinetic model [31] shown in Equations (29)–(31), and the kinetic data were employed using the literature [34].

$$r_{CH_3OH} = K_A \frac{K_{CO} \left[f_{CO} f_{H_2}^{\frac{3}{2}} - \frac{f_{CH_3OH}}{K_A \sqrt{f_{H_2}}} \right]}{(1 + K_{CO} f_{CO} + K_{CO_2} f_{CO_2}) \left[f_{H_2} + (K_{H_2O} / \sqrt{K_{H_2}}) f_{H_2O} \right]} \quad (29)$$

$$r_{CO} = K_B \frac{K_{CO_2} \left[f_{CO_2} f_{H_2} - \frac{f_{H_2O} f_{CO}}{K_B} \right]}{(1 + K_{CO} f_{CO} + K_{CO_2} f_{CO_2}) \left[f_{H_2} + (K_{H_2O} / \sqrt{K_{H_2}}) f_{H_2O} \right]} \quad (30)$$

$$r_{CH_3OH} = K_C \frac{K_{CO_2} \left[f_{CO} f_{H_2}^{\frac{3}{2}} - f_{H_2O} f_{CH_3OH} / (f_{H_2}^{\frac{3}{2}} k_C) \right]}{(1 + K_{CO} f_{CO} + K_{CO_2} f_{CO_2}) \left[f_{H_2} + (K_{H_2O} / \sqrt{K_{H_2}}) f_{H_2O} \right]} \quad (31)$$

The crude methanol produced from the methanol synthesis reactor contains unreacted H_2 , CO_2 , and water, which need further separation by methanol distillation to obtain a high-purity methanol product. It is worth noting that by-products such as methyl formate and alcohol are not included in the synthesis of green methanol. Therefore, a single-column distillation process with a simple process and stable operation [35] is used to obtain green methanol with a purity of 99.9%.

2.6. Absorption Refrigeration System

A double-effect lithium bromide ARC was thermodynamically modeled as an integrated component of a multi-generation model. Such systems are receiving increasingly widespread attention because of their ability to utilize a wide range of low-grade thermal energy, the safety and non-toxicity of the process mass, low noise, and stable performance during load changes [36]. The double-effect lithium bromide ARC established in this paper consisted of the following components.

- High-pressure generator (HP generator): Heating of concentrated dilute lithium bromide solutions to produce high-temperature refrigerant vapor and concentrated lithium bromide solutions;
- Low-pressure generator (LP generator): Generating low-temperature refrigerant vapor into the condenser;
- Condenser: Condensing low-temperature refrigerant vapor into refrigerant water in the evaporator;
- Evaporator: Making the refrigerant water evaporate and absorb heat to supply low-temperature refrigerant water;
- Absorber: The concentrated solution of lithium bromide in the absorber absorbs the refrigerant vapor produced in the evaporator and transfers the absorbed heat to the external cooling water;

- High-temperature solution heat exchanger: The higher-temperature concentrated solution from the high-pressure generator exchanges heat with the lower-temperature dilute solution from the absorber;
- Low-temperature solution heat exchanger: The concentrated solution from the LP generator exchanges heat with the dilute solution.

The generator's heat supply is derived from ORC calculations. In addition, the working fluid flow stream that exits the generator, absorber, evaporator, and condenser is deemed to be in a saturated state. Based on the flow streams, it is assumed that the generator and absorber outlet streams are saturated liquid solutions, the evaporator outlet streams are in a saturated vapor state, and the flow stream from the condenser is in the saturated aqueous phase.

The performance of the ARC is evaluated using the energetic coefficients of performance. The energetic coefficients of performance (*COP*) can be defined as the ratio of the sum of the heat released from the evaporator and condenser to the heat released from the HP generator.

$$COP = \frac{Q_{evaporator} + Q_{condenser}}{Q_{HP\ generator}} \quad (32)$$

Table 3 shows the validation results of the performance of the ARC simulated in this study against the cycle process developed in the literature [37]. It can be seen that the performance factors calculated for both simulations are the same for similar operating conditions.

Table 3. Operating and design parameters for ARC.

Parameters	Unit	This Work	Reference [37]
Pressure in HP generator	kPa	7.777	7.777
Pressure in LP generator	kPa	93	92.6
Weak solution concentration in the absorber	Mass%	57.52	57.67
Strong solution concentration in HP generator	Mass%	60.19	60.37
Strong solution concentration in LP generator	Mass%	63.82	62.92
Refrigerant temperature in evaporator	°C	5	5
COP	-	1.45	1.45

3. Thermodynamic and Economic Analysis

3.1. Thermodynamic Analysis

The energy analysis of a system is a necessary part of the energy conversion process, reflecting the overall energy use of the system's input energy. According to the first law of thermodynamics, energy efficiency is defined as the ratio of the target product energy to the input energy, as seen in Equation (33). The input energy for chemical processes includes the energy of the raw material, electricity, water, steam, catalyst, solvent, or other components.

$$\eta_{energy} = \frac{W_{net} + Q_{HW} + Q_{cooling} + E_p - E_f}{Q_{solar}} \quad (33)$$

where η represents the energy efficiency, W_{net} represents the net power generation, Q_{HW} , $Q_{cooling}$ represent the energy of the domestic hot water and cooling systems respectively, E_p represents the energy of the system product, and E_f represents the energy of the feed.

The exergy is the maximum amount of work a system can achieve given the environmental conditions. It is based on the first and second laws of thermodynamics. It uses the equilibrium of the heat of the processing system to analyze the transfer, conversion, and utilization of the energy in the system. It is based on the first and second laws of thermodynamics. It uses the balance of the processing system to analyze the loss and utilization of "mass" during the transfer, conversion, and utilization of the system's energy, thus clearly identifying the processing system's weak points and optimization potential [38]. The base-line ambient state is assumed to be 1 atm and 25 °C, and kinetic and potential energy are

ignored before performing the analysis. Therefore, the logistic energy, considering only physical and chemical energy, can be calculated by the following equation.

$$e = e_{ph} + e_{ch} \quad (34)$$

where e_{ph} represents the physical exergy, e_{ch} represents the chemical exergy.

As shown in Equation (35), the physical exergy is calculated by the entropy and enthalpy values in the base state, and the parameters related to the physical exergy of the logistics can be calculated using the built-in module of Aspen Plus.

$$e_{ph} = H - H_0 - T_0(S - S_0) \quad (35)$$

In addition, the chemical exergy of non-gaseous and gaseous mixtures is defined by the following equations [39].

$$e_{ch} = \sum_i n_i e_{stand} \quad (36)$$

$$e_{ch} = \sum_i x_i e_{stand} + RT_0 \sum_i x_i \ln x_i \quad (37)$$

where n_i represents the molar flow rate of a component in the stream, x_i is the molar fraction of the component. R is the gas constant. e_{stand} represents the standard chemical exergy value of the component.

In an irreversible process, energy changes occur, and the total exergy is reduced and irreversible, called exergy destruction. The exergy destruction can be calculated by the following equation.

$$E_{des} = T_0 S_{generation} \quad (38)$$

Therefore, the complete exergy balance can be calculated by the following equations.

$$W + \sum E_{x_{Qin}} + \sum E_{xin} = \sum E_{x_{Qout}} + \sum E_{xout} + E_{des} \quad (39)$$

$$E_{x_Q} = \sum_i \left[\left(1 - \frac{T_0}{T_i} \right) Q_i \right] \quad (40)$$

where W is the power or mechanical work supplied, equal to the exergy input. $\sum E_{xin}$ and $\sum E_{xout}$ represent the exergy of outflow and inflow systems, respectively, while $\sum E_{x_{Qin}}$ and $\sum E_{x_{Qout}}$ represent the actual heat and cold sources, respectively. Both depend on the heating temperature and the transfer heat load Q_i , which can be calculated from Equation (40).

Finally, the exergy efficiency of a typical chemical process is defined as the ratio of the output exergy to the input exergy.

$$\eta_{exergy} = \frac{E_{x_{product}}}{E_{x_{sloar}} + E_{x_{add}}} \quad (41)$$

3.2. Economic Analysis

This paper uses capital costs (CC) and operating costs (OC) to analyze the economics of the system. CC includes a direct capital cost (DC), indirect capital cost (IDC), working capital (WC), and land costs (LC) for setting up the processing system for all equipment units. OC includes transportation costs (TC), raw material costs (MC), utility costs (UC), operations and maintenance costs (O&M), property taxes and insurance (PT&I), general expenses (GC), and income taxes (IT). They are calculated respectively by the following equations.

$$CC = DC + IDC + WC + LC \quad (42)$$

$$OC = TC + MC + UC + O\&M + TC + PT\&I + GC + IT \quad (43)$$

For the *CC* estimate, *DC* consists of equipment purchase costs (*EPC*) and installation costs (*IC*), with *IC* estimated to be 55% of the *EPC*. *IDC* and *LC* were estimated at 123% and 6% of the total *EPC*. *WC* was estimated at 5% of the combined *IC* and *LC*. *TC* was estimated mainly based on the weight and distance of the product transported for *OC* estimation. Considering the location of the plant is remote, the transportation cost was calculated using 1.2 times the average unit transportation cost in Beijing, which is 0.12\$/ (t*km). The rest of the specific costs were calculated using the literature [40].

The project's net present value (*NPV*) can be obtained by combining the operating cost and the cost of capital. Due to the effects of time and inflation, cash flows now are more valuable than future ones. Therefore, subtracting the discounted cash inflows obtained in the future from the initial cash outlay required for the investment gives the *NPV* as shown in Equation (44).

$$NPV = \sum_i^{Life\ cycle} \frac{AR}{(1 + Dr)^i} - CC \quad (44)$$

where *AR* represents the annual revenue of a project as the difference between annual product income and *OC*. The discount rate (*Dr*) is set at 10% for process updates with a 20-year lifespan. When the *NPV* of a project is more than zero, it is very financially beneficial. Moreover, the internal rate of return (*IRR*) simplifies the evaluation of the investment potential of a project under diverse circumstances. The *IRR* calculation has been shown in Equation (45) and it stands for the discount rate that makes the *NPV* of all cash flows equal to zero. If the *IRR* is more than the real discount rate, the project's economic viability appears promising.

$$\sum_i^{Life\ cycle} \frac{AR}{(1 + IRR)^i} = CC \quad (45)$$

4. Result and Discussion

4.1. Parametric Analysis

The system's main energy source is solar energy, which is absorbed through PTC and combined with the ORC to generate electricity. Therefore, the selection of the PTC site, the circulating heat exchange fluid in the PTC, the circulating mass in the ORC, and the inlet temperature and pressure of the ORC expander significantly impact the power generation.

Dunhuang, situated in North-western China, has a longitude of 94.66° and a latitude of 40.14°. The dry climate with sufficient sunshine hours makes it a logical choice for the construction and design of PTC collector fields. The modeling of the PTC collector system was implemented using MATLAB, and the variation of the main parameters with local time, such as solar radiation, angle of incidence, optical efficiency, thermal efficiency, working fluid exit temperature, and adequate energy gained by the working fluid, was investigated for the performance of the PTC system.

A critical factor in the operation of the PTC is the amount of solar radiation it receives, as shown in Figure 3a. Solar radiation changes dramatically with time during the day, reaching a maximum at midday local time, when the angle of incidence of the sun is at its minimum. Variations in the incidence angle and the intensity of solar radiation cause changes in the optical and thermodynamic efficiency of the collector, as shown in Figure 3b. The day with the strongest solar radiation is chosen as the object of study. The changes in the collector's optical and thermodynamic efficiency and the solar radiation intensity are positively and negatively correlated with the changes in the angle of incidence. Due to the instability of solar radiation, it is necessary to increase the circulation of the heat transfer fluid within the collector tube. Auxiliary heaters need to be activated where necessary to meet the stable PTC outlet temperature (310 °C) and to achieve a stable heat supply to the ORC system. The performance of the auxiliary heaters is beyond the scope of this paper and is not explicitly analyzed.

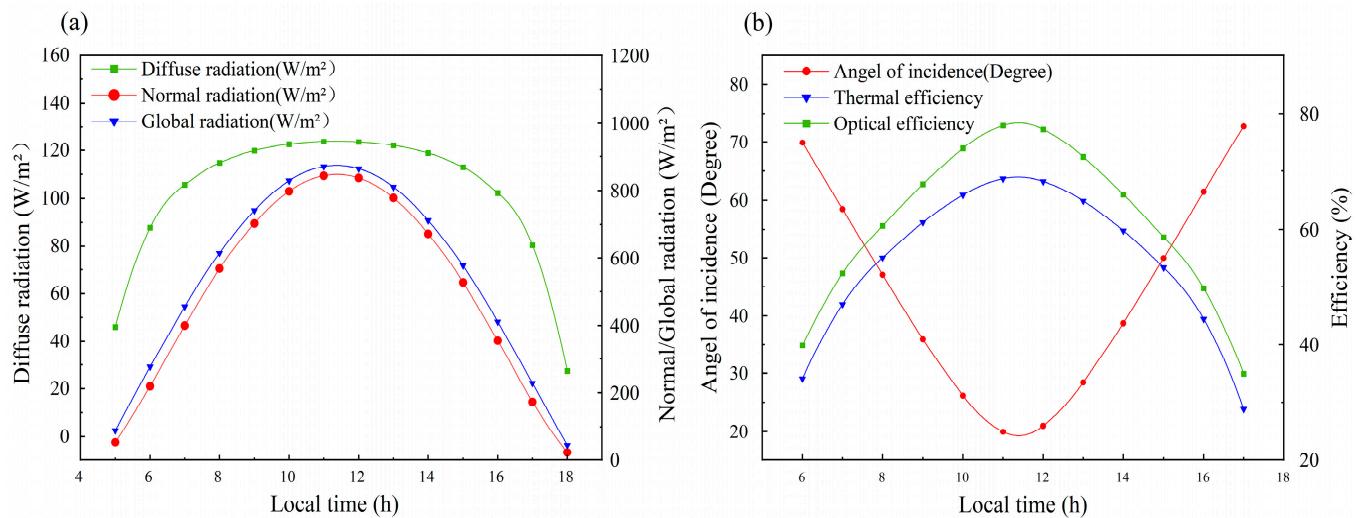


Figure 3. (a) Hourly solar radiation in Dunhuang; (b) hourly optical and thermal efficiency of PTC system.

The regenerative extraction ORC established in this paper extracts part of the un-expanded high-temperature and high-pressure organic steam in the expander to heat the low-temperature fluid at the pump outlet to improve the system's thermal efficiency. The key parameters to evaluate the performance of the regenerative extraction ORC are the extraction ratio, the extraction pressure, and the inlet temperature of the expander. These three parameters have a significant impact on the output power and efficiency of the system.

Depending on the temperature range of the heat source, six working mediums, R113, R123, R134a, R141b, R245fa, and R601a, were studied in this paper. Figure 4a represents the effect of the extraction ratio on the thermal efficiency of the regenerative extraction ORC. As the extraction ratio increases, both the heat absorption and the net output power in the evaporator decrease, but the net output power decreases to a greater extent, so the system thermal efficiency increases, and the extraction of gas reheat can effectively improve the system thermal efficiency. Figure 4b shows the effect of pumping pressure on the thermal efficiency of the regenerative extraction ORC. The thermal efficiency of the work system tends to increase with increasing pumping pressure. The rate of increase in net output work exceeds the rate of increase in heat absorption, and the system's thermal efficiency increases.

Figure 4c shows the effect of expander inlet temperature on the net output power of the ORC for different fluid cases. As the temperature increases, the net output power of the system also increases, while the heat load on the evaporator increases, which leads to a slight reduction in the cycle thermal efficiency. The R601a produces the highest power generation among the selected working mediums in the high-temperature heat source case. Therefore, considering the power generation capacity of different mediums at the same flow rate, R601a was selected as the circulating medium for the ORC, and the optimum pumping ratio and pumping pressure were determined to be 15% and 25 bar, respectively.

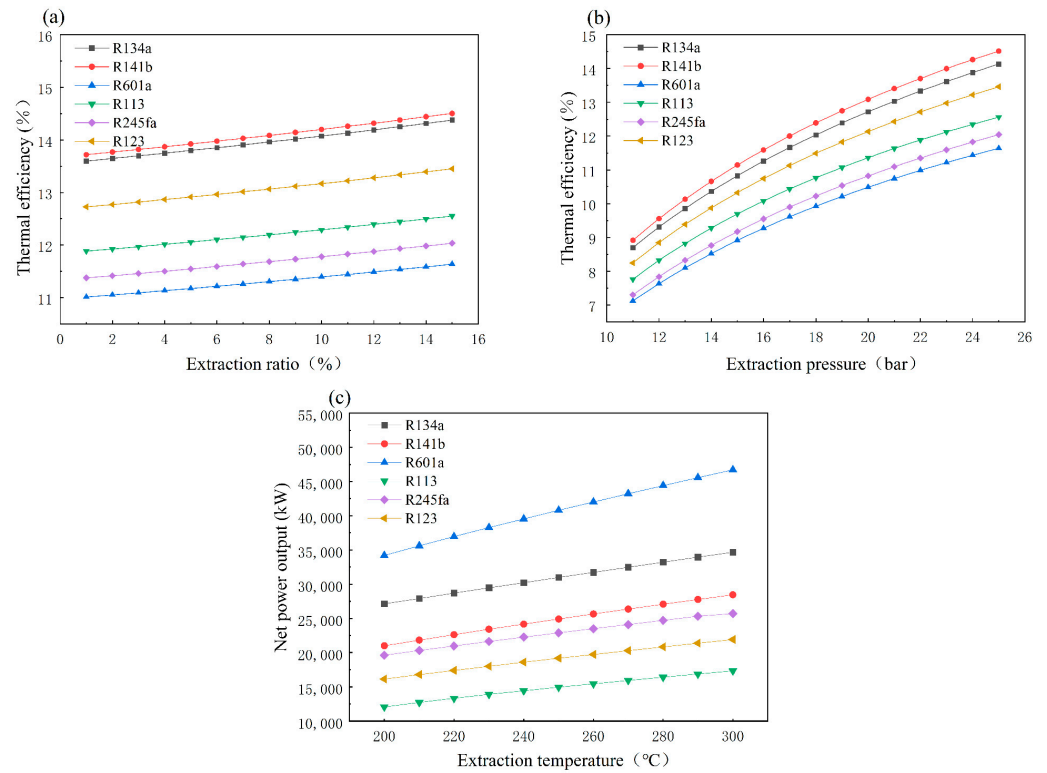


Figure 4. (a) Effect of extraction ratio on the thermal efficiency of the regenerative extraction ORC; (b) effect of pumping pressure on the thermal efficiency of the regenerative extraction ORC; (c) effect of expander inlet temperature on the net output power of the ORC.

4.2. Thermodynamic Analysis Results

After determining the working fluid and operating conditions of the PTC and ORC, an energy analysis was carried out. Wang [41] proposed a method of combining green hydrogen production (GH) with the CO₂ utilization of the coal-to-methanol process (CTM) and analyzed the energy efficiency of conventional CTM and GH-CTM. As shown in Figure 5, the integrated system proposed in this paper has a high energy efficiency due to the reduced utility energy consumption. Reducing the energy consumption for hydrogen production is one of the critical ways to improve the energy efficiency of the process further, so the development of new electrolytic water catalysts is necessary.

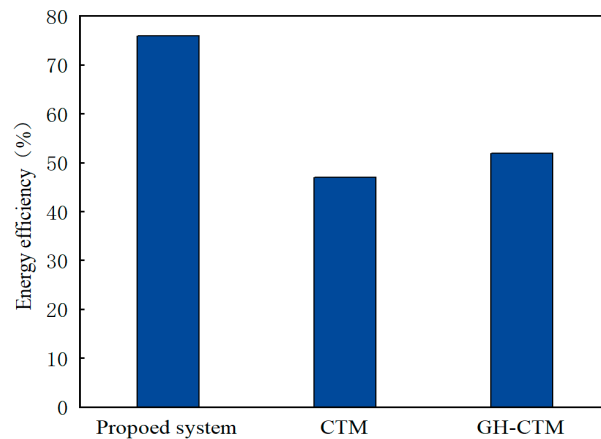


Figure 5. Energy efficiency of the proposed process, CTM, GH-CTM process.

Figure 6 depicts the exergy streams flow for the suggested processes, with methanol as the main target product and a total exergy input of 316.8 MW and exergy efficiency of

22.8%. The main reason for the low heat efficiency is the high exergy destruction (132.6 MW) from the PTC system, which accounts for 57.6% of the total exergy destruction. It can be attributed to the irreversible nature of heat transfer and the high entropy yield. The ORC system (69.706 MW) and the electrolyzer (20.142 MW) accounted for 30.3% and 8.7% of the total heat loss, respectively. High exergy destruction created by heat exchangers is the primary source of exergy destruction in the ORC system. The detailed distribution of exergy destruction is given in Figure 7. It can be seen that the heat exchanger has the highest exergy destruction of all equipment except the PTC system, accounting for 26.1% of the total equipment exergy destruction. In conclusion, the optical and thermal efficiency can be improved by researching and upgrading solar collectors to reduce exergy damage and thus further improve the exergy efficiency of the system.

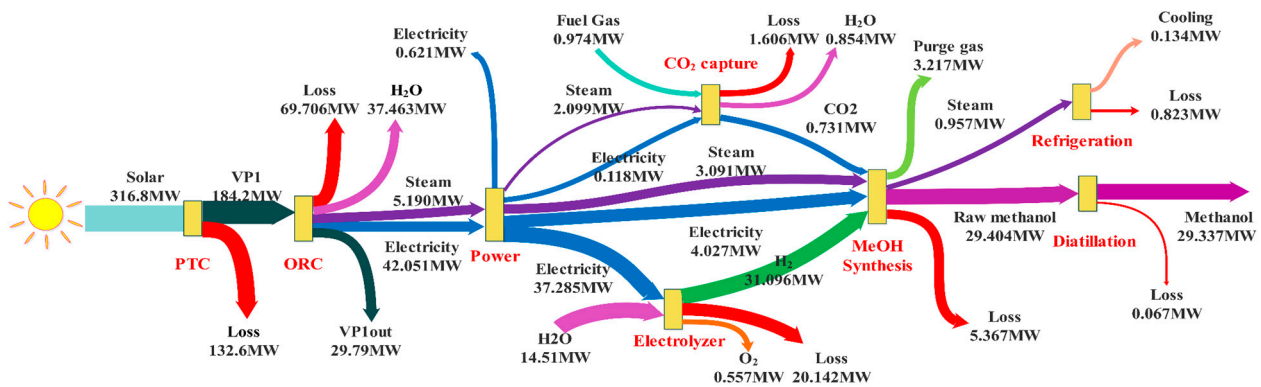


Figure 6. The exergy flow of the proposed green poly-generation integrated system.

- Flashes & Valves & Reactors
- Towers
- Compressors & Turbines & Pumps
- Alkaline Electrolyzer
- Heat Exchangers
- Parabolic trough collectors

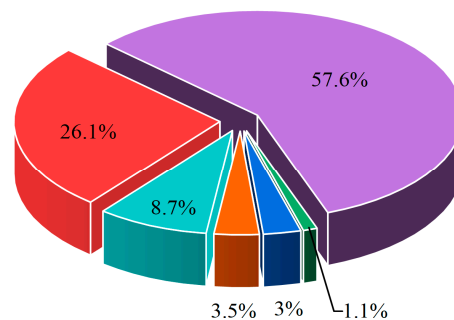


Figure 7. The pie chart of the equipment's contributions to the overall exergy destruction.

4.3. Economic Results

A sensitivity analysis of the economic evaluation indicators presented above was used to evaluate whether the proposed process is promising and economically viable for application. The economic analysis considered the cost of electricity (utility costs) required to support the process cycle using grid input power when solar energy is unavailable at night and on cloudy days. The main cost analysis for the project is shown in Figure 8, where the OC for the project is only 16.71% of the total cost. However, the CC is 83.29% of the total cost, which does not exactly match the reality of the chemical plant. The main reason is the higher equipment costs for the PTC and ORC. The higher equipment costs for the PTC are mainly due to the higher number of collectors and the high collector cost, while the ORC system contains several expensive expanders and heat exchangers. The project's

direct costs are higher (the sum of equipment and installation costs), raising the CC share of the total costs. At the same time, the project’s indirect costs account for 35.7% of the total costs and are mainly made up of miscellaneous costs, site costs, and welfare allowances. The small pie chart on the right indicates the breakdown of CC, with the highest share of electricity consumption and depreciation costs for solar collector farms at night, at 4.42% and 3.33%, respectively.

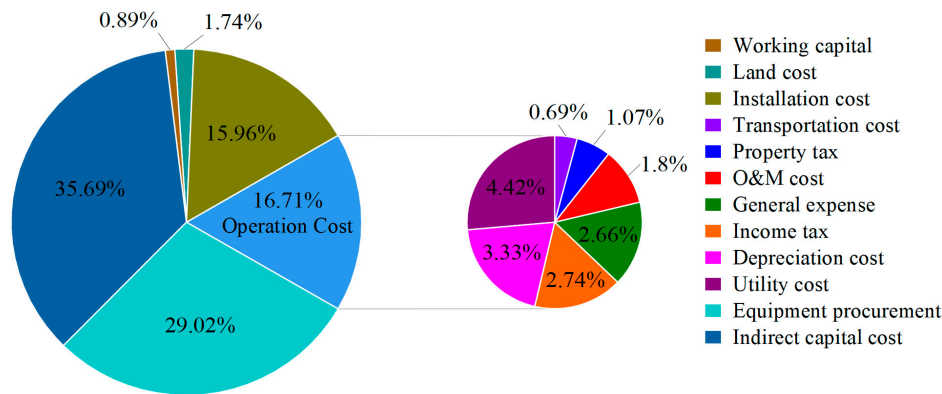


Figure 8. Economic cost breakdown for the proposed green poly-generation integrated system.

Figure 9a reflects the impact of the discount rate on NPV. Typically, an IRR of 10% can be used as a better value to assess the economic viability of a project, taking into account monetary inflation. If the discount rate is much greater than 10%, then the total cash flows over the life cycle will be negative, which means the project will not be feasible to implement. When the discount rate is 10%, the NPV of the project is positive, while the IRR is calculated to be 11.394%, which represents the threshold value of the discount rate that makes the NPV equal to zero. As mentioned earlier, when the IRR is greater than the actual discount rate, the project can be considered to be economically viable.

Methanol is considered the system’s main product, and the cost of green methanol production for the proposed multi-coupling process is 1539.26 \$/ton. This value is in line with the recent IRENA summary report (i.e., 820–1620 \$/ton) [42]. The cost of green methanol depends mainly on the cost of H₂ and CO₂. The cost of CO₂ will depend on the source of access (biological, DAC, industrial). The cost of H₂ is closely related to the cost of electricity to produce H₂, the utilization of the electrolyzer unit, and its cost. With approximately 50 MWh of electricity required to produce each ton of H₂, reducing the cost of electricity is the first driver for reducing the cost of green methanol. In addition to the cost of electricity, the cost of the electrolyzer needs to be further reduced and there should be a large amount of affordable renewable CO₂ available. As mentioned above, the higher equipment costs of PTC and ORC lead to higher electricity costs for hydrogen production, increasing the cost of methanol production.

In addition to methanol, the system also produces by-products, such as O₂ from the electrolyzer, a large amount of domestic hot water from the heat exchange process, and refrigeration from the absorption refrigeration system. The pressure on the production costs of methanol can be effectively relieved. Carbon credits can significantly impact the cost of the green methanol produced. 100 \$/ton of CO₂ carbon credits can reduce the cost of methanol by 172 \$/ton compared to no carbon credits. The future availability of carbon credits will play an essential role in improving the competitiveness of the renewable methanol [42].

At the same time, due to the volatility of the market price of methanol, the economic returns of the plant can also be effectively increased by selling by-products. As shown in Figure 9b, when the methanol price fluctuates between 300 to 500 \$/ton, the economic indicator IRR is more volatile and the impact of methanol price fluctuation on annual revenue (AR) is less due to the presence of by-products. The base methanol price was set at

450 \$/ton. The analysis in Figure 9b shows that the project is economically viable when the methanol price exceeds 363.34 \$/ton. As the price of methanol rises, the profitability of the project becomes more implausible.

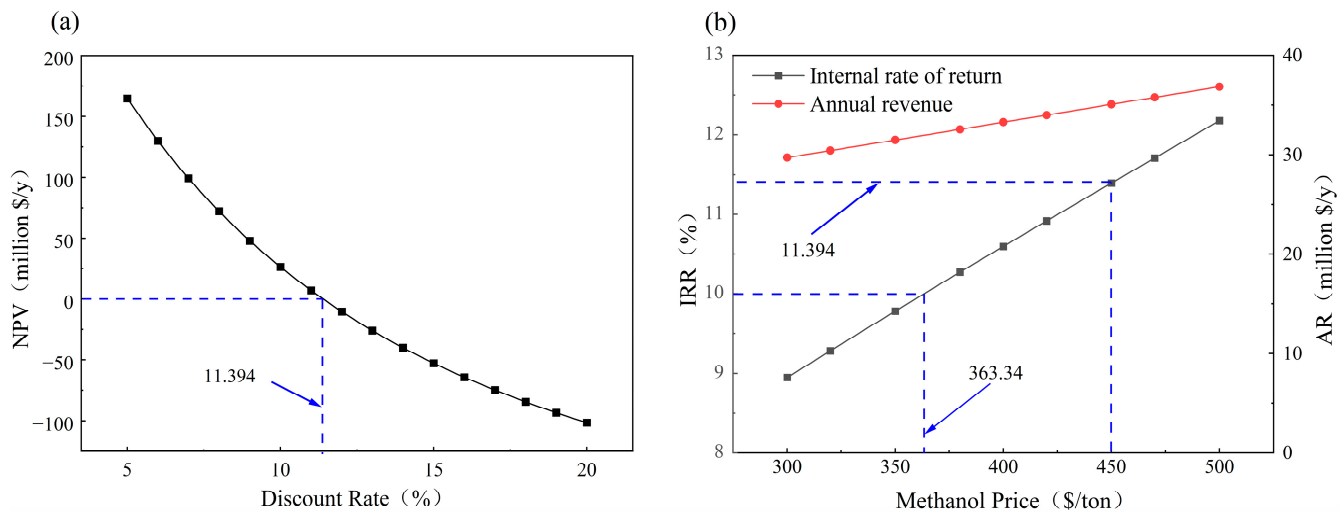


Figure 9. (a) The effect of discount rate on the NPV of the project in 20 years life span; (b) Impact of methanol prices on the final IRR and AR of the project.

5. Conclusions

In this study, a green poly-generation integrated system with green methanol as the main product was designed and proposed for the production of domestic hot water, O₂, and cooling at the same time. The proposed green poly-generation integrated system consisted of six different operating units which were integrated to exchange heat and energy. The operating units were: (1) parabolic trough solar collector system; (2) organic Rankine cycle; (3) CO₂ capture unit; (4) alkaline electrolysis unit; (5) green methanol synthesis and distillation unit; (6) double-effect lithium bromide absorption refrigeration cycle. The parabolic trough solar collector system supplied the thermal energy necessary to operate the organic Rankine cycle, which provided the necessary power for all operating units. The H₂ and CO₂ required for green methanol synthesis came from the alkaline electrolyzer and the MEA-based CO₂ capture system. The alkaline electrolyzer also produced O₂ as a by-product. In addition, domestic hot water and cooling were generated in the system's heat exchange network and lithium bromide double-effect absorption refrigeration cycle, respectively. The system was evaluated based on energy and exergy analysis, while the feasibility of the system was assessed using economic analysis. The main results and findings of the study can be summarized as follows:

(1) The proposed plant can produce 147.4 kmol/h of green methanol at 99.99% purity with a by-production of 230.6 kmol/h of O₂, 283,500 kmol/h of domestic hot water, and 1341 kW of cooling;

(2) The results of the energy and exergy analysis show that the energy efficiency and exergy efficiency of the system can reach 76% and 22.8%, respectively. The solar collector system and heat exchanger contribute the most to the equipment's exergy destruction with 57.6% and 26.1%, respectively;

(3) Six working mediums, R113, R123, R134a, R141b, R245fa, and R601a, were studied for the regenerative extraction organic Rankine cycle system. The R601a has a higher power generation than the other working medium, and the thermal efficiency of the ORC system increases with both the extraction ratio and the extraction pressure;

(4) Without subsidies, the IRR of the system is 11.394%. While the average IRR value is 10% so that the system can be economically viable. The average production cost of green methanol is 1539.26 \$/ton. The presence of by-products such as O₂ and domestic hot water can reduce the average production cost of green methanol. Analysis of the

methanol price shows that the project is economically viable when the methanol price exceeds 363.34 \$/ton.

The main barrier to green methanol production is the cost of providing H₂ through the energy-intensive water electrolysis process. The proposed poly-generation integrated system in this paper uses solar collectors to provide energy for the ORC to generate electricity to power the electrolyzer. However, the equipment investment for solar collectors is high. At the same time, the operation of the solar collectors produces dynamic fluctuations due to thermal efficiency and natural environmental variations. Therefore, the application of fuel cell storage technology and molten salt heat storage technology in the multi-coupling system proposed in this paper can be further investigated.

Author Contributions: Conceptualization, Q.Y.; methodology, Y.B.; software, Y.B.; validation, Q.Y. and Y.L.; writing—original draft preparation, Y.B.; writing—review and editing, Q.Y. and H.P.; visualization, Y.B.; supervision, P.Y. All authors have read and agreed to the published version of the manuscript.

Funding: This research received no external funding.

Data Availability Statement: Not applicable.

Acknowledgments: This work was financially supported by the National Natural Science Foundation of China [Nos. 22178113].

Conflicts of Interest: The authors declare no conflict of interest.

References

1. Bakhtyari, A.; Mofarahi, M.; Lee, C.-H. CO₂ adsorption by conventional and nanosized zeolites. In *Advances in Carbon Capture*; Woodhead Publishing: Sawston, UK, 2020; pp. 193–228.
2. Chen, J.M. Carbon neutrality: Toward a sustainable future. *Innovation* **2021**, *2*, 100127. [[CrossRef](#)] [[PubMed](#)]
3. IPCC Global Warming of 1.5 °C. An IPCC Special Report on the Impacts of Global Warming of 1.5 °C above Pre-industrial Levels and Related Global Greenhouse Gas Emission Pathways, in the Context of Strengthening the Global Response to the Threat of Climate Change. Available online: <https://www.ipcc.ch/sr15/> (accessed on 10 July 2022).
4. Kauw, M.; Benders, R.M.; Visser, C. Green methanol from hydrogen and carbon dioxide using geothermal energy and/or hydropower in Iceland or excess renewable electricity in Germany. *Energy* **2015**, *90*, 208–217. [[CrossRef](#)]
5. Lacerda de Oliveira Campos, B.; John, K.; Beeskow, P.; Herrera Delgado, K.; Pitter, S.; Dahmen, N.; Sauer, J. A Detailed Process and Techno-Economic Analysis of Methanol Synthesis from H₂ and CO₂ with Intermediate Condensation Steps. *Processes* **2022**, *10*, 1535. [[CrossRef](#)]
6. Van-Dal, S.; Bouallou, C. Design and simulation of a methanol production plant from CO₂ hydrogenation. *J. Clean. Prod.* **2013**, *57*, 38–45. [[CrossRef](#)]
7. Kumar, K.; Alam, M.; Verma, S.; Dutta, V. Effect of hysteresis band control strategy on energy efficiency and durability of solar-hydrogen storage based microgrid in partial cloudy condition. *J. Energy Storage* **2020**, *32*, 101936. [[CrossRef](#)]
8. Khairat Dawood, M.M.; Nabil, T.; Kabeel, A.E.; Shehata, A.I.; Abdalla, A.M.; Elnaghi, B.E. Experimental study of productivity progress for a solar still integrated with parabolic trough collectors with a phase change material in the receiver evacuated tubes and in the still. *J. Energy Storage* **2020**, *32*, 102007. [[CrossRef](#)]
9. Atmane, I.; El Moussaoui, N.; Kassmi, K.; Deblecker, O.; Bachiri, N. Development of an Innovative Cooker (Hot Plate) with Photovoltaic Solar Energy. *J. Energy Storage* **2021**, *36*, 102399. [[CrossRef](#)]
10. Senthil, R.; Cheralathan, M. Enhancement of the thermal energy storage capacity of a parabolic dish concentrated solar receiver using phase change materials. *J. Energy Storage* **2019**, *25*, 100841. [[CrossRef](#)]
11. Huang, W.; Marefati, M. Energy, exergy, environmental and economic comparison of various solar thermal systems using water and Therminol base fluids, and CuO and Al₂O₃ nanofluids. *Energy Rep.* **2020**, *6*, 2919–2947. [[CrossRef](#)]
12. Behar, O.; Khellaf, A.; Mohammedi, K. A novel parabolic trough solar collector model—Validation with experimental data and comparison to Engineering Equation Solver (EES). *Energy Convers. Manag.* **2015**, *106*, 268–281. [[CrossRef](#)]
13. Shahin, M.S.; Orhan, M.F.; Uygul, F. Thermodynamic analysis of parabolic trough and heliostat field solar collectors integrated with a Rankine cycle for cogeneration of electricity and heat. *Sol. Energy* **2016**, *136*, 183–196. [[CrossRef](#)]
14. Petrollese, M.; Cocco, D. Robust optimization for the preliminary design of solar organic Rankine cycle (ORC) systems. *Energy Convers. Manag.* **2019**, *184*, 338–349. [[CrossRef](#)]
15. Martín, M. Methodology for solar and wind energy chemical storage facilities design under uncertainty: Methanol production from CO₂ and hydrogen. *Comput. Chem. Eng.* **2016**, *92*, 43–54. [[CrossRef](#)]
16. El-Emam, R.S.; Dincer, I. Investigation and assessment of a novel solar-driven integrated energy system. *Energy Convers. Manag.* **2018**, *158*, 246–255. [[CrossRef](#)]

17. Mehrpooya, M.; Ghorbani, B.; Hosseini, S.S. Thermodynamic and economic evaluation of a novel concentrated solar power system integrated with absorption refrigeration and desalination cycles. *Energy Convers. Manag.* **2018**, *175*, 337–356. [[CrossRef](#)]
18. Liu, X.; Yang, X.; Yu, M.; Zhang, W.; Wang, Y.; Cui, P.; Zhu, Z.; Ma, Y.; Gao, J. Energy, exergy, economic and environmental (4E) analysis of an integrated process combining CO₂ capture and storage, an organic Rankine cycle and an absorption refrigeration cycle. *Energy Convers. Manag.* **2020**, *210*, 112738. [[CrossRef](#)]
19. Liu, X.; Liang, J.; Xiang, D.; Yang, S.; Qian, Y. A proposed coal-to-methanol process with CO₂ capture combined Organic Rankine Cycle (ORC) for waste heat recovery. *J. Clean. Prod.* **2016**, *129*, 53–64. [[CrossRef](#)]
20. Chein, R.-Y.; Chen, W.-H.; Ong, H.C.; Show, P.L.; Singh, Y. Analysis of methanol synthesis using CO₂ hydrogenation and syngas produced from biogas-based reforming processes. *Chem. Eng. J.* **2021**, *426*, 130835. [[CrossRef](#)]
21. Battaglia, P.; Buffo, G.; Ferrero, D.; Santarelli, M.; Lanzini, A. Methanol synthesis through CO₂ capture and hydrogenation: Thermal integration, energy performance and techno-economic assessment. *J. CO₂ Util.* **2020**, *44*, 101407. [[CrossRef](#)]
22. Vo, T.T.; Wall, D.M.; Ring, D.; Rajendran, K.; Murphy, J.D. Techno-economic analysis of biogas upgrading via amine scrubber, carbon capture and ex-situ methanation. *Appl. Energy* **2018**, *212*, 1191–1202. [[CrossRef](#)]
23. Sun, K.; Zhao, T.; Wu, S.; Yang, S. Comprehensive evaluation of concentrated solar collector and Organic Rankine cycle hybrid energy process with considering the effects of different heat transfer fluids. *Energy Rep.* **2021**, *7*, 362–384. [[CrossRef](#)]
24. White, C.W. *ASPEN Plus Simulation of CO₂ Recovery Process*; DOE/NETL-2002/1182; NETL: Pittsburgh, PA, USA, 2002.
25. Akinola, T.E.; Oko, E.; Wang, M. Study of CO₂ removal in natural gas process using mixture of ionic liquid and MEA through process simulation. *Fuel* **2018**, *236*, 135–146. [[CrossRef](#)]
26. Zacchello, B.; Oko, E.; Wang, M.; Fethi, A. Process simulation and analysis of carbon capture with an aqueous mixture of ionic liquid and monoethanolamine solvent. *Int. J. Coal Sci. Technol.* **2016**, *4*, 25–32. [[CrossRef](#)]
27. Knudsen, J.N.; Jensen, J.N.; Vilhelmsen, P.-J.; Biede, O. Experience with CO₂ capture from coal flue gas in pilot-scale: Testing of different amine solvents. *Energy Procedia* **2009**, *1*, 783–790. [[CrossRef](#)]
28. Duan, L.; Zhao, M.; Yang, Y. Integration and optimization study on the coal-fired power plant with CO₂ capture using MEA. *Energy* **2012**, *45*, 107–116. [[CrossRef](#)]
29. Ursua, A.; Gandia, L.M.; Sanchis, P. Hydrogen Production from Water Electrolysis: Current Status and Future Trends. *Proc. IEEE* **2012**, *100*, 410–426. [[CrossRef](#)]
30. Van-Dal, É.S.; Bouallou, C. CO₂ Abatement Through a Methanol Production Process. *Chem. Eng. Trans.* **2012**, *29*, 463–468.
31. Xin, A.; Yizan, Z.; Qiang, Z.; Jinfu, W.A. Methanol Synthesis from CO₂ Hydrogenation with a Cu/Zn/Al/Zr Fibrous Catalyst. *Chin. J. Chem. Eng.* **2009**, *17*, 88–94.
32. Wang, D.; Li, J.; Meng, W.; Wang, J.; Wang, K.; Zhou, H.; Yang, Y.; Fan, Z.; Fan, X. Integrated Process for Producing Glycolic Acid from Carbon Dioxide Capture Coupling Green Hydrogen. *Processes* **2022**, *10*, 1610. [[CrossRef](#)]
33. Lim, H.-W.; Park, M.-J.; Kang, S.-H.; Chae, H.-J.; Bae, J.W.; Jun, A.-W. Modeling of the Kinetics for Methanol Synthesis using Cu/ZnO/Al₂O₃/ZrO₂ Catalyst: Influence of Carbon Dioxide during Hydrogenation. *Ind. Eng. Chem. Res.* **2009**, *48*, 10448–10455. [[CrossRef](#)]
34. Kiss, A.A.; Pragt, J.J.; Vos, H.J.; Bargeman, G.; de Groot, M.T. Novel efficient process for methanol synthesis by CO₂ hydrogenation. *Chem. Eng. J.* **2016**, *284*, 260–269. [[CrossRef](#)]
35. Milani, D.; Khalilpour, R.; Zahedi, G.; Abbas, A. A model-based analysis of CO₂ utilization in methanol synthesis plant. *J. CO₂ Util.* **2015**, *10*, 12–22. [[CrossRef](#)]
36. Mussati, S.F.; Cignitti, S.; Mansouri, S.S.; Gernaey, K.V.; Morosuk, T.; Mussati, M.C. Configuration optimization of series flow double-effect water-lithium bromide absorption refrigeration systems by cost minimization. *Energy Convers. Manag.* **2018**, *158*, 359–372. [[CrossRef](#)]
37. Zhou, C.; Lv, F.; Wan, Z.; Wang, Y.; Luo, C. A double-effect/two-stage absorption refrigeration and thermal energy storage hybrid cycle using dual working fluids. *Appl. Therm. Eng.* **2022**, *214*, 118858. [[CrossRef](#)]
38. Li, G.; Liu, Z.; Liu, F.; Yang, B.; Ma, S.; Weng, Y.; Zhang, Y.; Fang, Y. Advanced exergy analysis of ash agglomerating fluidized bed gasification. *Energy Convers. Manag.* **2019**, *199*, 111952. [[CrossRef](#)]
39. Niasar, M.S.; Amidpour, M. Conceptual design and exergy analysis of an integrated structure of natural gas liquefaction and production of liquid fuels from natural gas using Fischer-Tropsch synthesis. *Cryogenics* **2018**, *89*, 29–41. [[CrossRef](#)]
40. Zhao, X.; You, F. Waste respirator processing system for public health protection and climate change mitigation under COVID-19 pandemic: Novel process design and energy, environmental, and techno-economic perspectives. *Appl. Energy* **2020**, *283*, 116129. [[CrossRef](#)]
41. Dongliang, W.; Wenliang, M.; Huairong, Z.; Guixian, L.; Yong, Y.; Hongwei, L. Green hydrogen coupling with CO₂ utilization of coal-to-methanol for high methanol productivity and low CO₂ emission. *Energy* **2021**, *231*, 120970. [[CrossRef](#)]
42. Irena And Methanol Institute. *Innovation Outlook: Renewable Methanol*, International Renewable Energy Agency; Irena And Methanol Institute: Abu Dhabi, United Arab Emirates, 2021.

Disclaimer/Publisher’s Note: The statements, opinions and data contained in all publications are solely those of the individual author(s) and contributor(s) and not of MDPI and/or the editor(s). MDPI and/or the editor(s) disclaim responsibility for any injury to people or property resulting from any ideas, methods, instructions or products referred to in the content.